A Suboptimal Discrete-Time Predictive Current Controller for a Voltage-Source Inverter

Shahab Kaynama and Osman Kükrer

***Abstract*— This paper presents a discrete-time predictive control strategy for a voltage-source inverter based on computation of a deadbeat control law and its approximating suboptimal voltage vector at every sampling interval. The controller, in addition to compensating for the inherent delay in the system, employs a simple prediction filter to suppress the disturbance caused by the back-EMF voltages and improve robustness against parameter variations across the load. Discussions on the effect of the back-EMF prediction on the performance and robustness of the system is provided. It is shown that the proposed control strategy yields satisfactory transient and steady-state behavior and that the closed-loop system can tolerate a wide range of parameter variations and model uncertainty.**

Keywords: **predictive control, current control, digital control, inverter**

I. Introduction

In the past two decades the predictive current control of voltage-source inverters (VSI) has gained significant attention among researchers (see [1] for an excellent survey). The recent emergence of fast microprocessors has enabled the use of various control strategies within the predictive control framework ranging from relatively simple-to-implement model-based approaches to more sophisticated and computationally demanding adaptive schemes (see [2]–[17] and the references therein).

Depending on the type of controller, appropriate gate signals are synthesized and applied to the inverter (directly or indirectly through e.g. pulsewidth modulation (PWM) techniques and a gate drive circuitry) such that the resulting voltage waveform at the output of the inverter generates a load current that satisfies some performance criteria (e.g. tracking a reference signal).

In particular, discrete-time predictive control strategies have seen wide-spread application due to their digitally implementable nature, intuitive structure, and constant switching frequency under all operating conditions. This approach is based on the discretization of the ordinary differential equations that model the inverter-load system. The voltage required by the load to achieve a desired current is computed according to this discrete-time model. Advanced techniques such as space-vector modulation can then be used to realize this pre-computed voltage.

S. Kaynama is a graduate student with the Department of Electrical and Computer Engineering, University of British Columbia, Vancouver, BC, Canada kaynama@ece.ubc.ca

O. Kükrer is a Professor with the Department of Electrical and Electronic Engineering, Eastern Mediterranean University, Gazi Magusa, Turkey osman.kukrer@emu.edu.tr

In [15] a very effective (yet computationally simple) algorithm is presented. The discrete-time model of the system is used to predict the value of the load current for each switching state of the inverter. The switching state that minimizes a cost function (in this case defined as the error between reference and actual output currents) is then selected and sent directly to the inverter gates. It is shown that the use of this technique can waive the need for more complex modulation techniques and that the switching frequency is limited, by construction, to half the sampling frequency.

In this paper we present a predictive control strategy based on computing an optimal deadbeat control input (i.e. an input that eliminates the output error at every time step) and its suboptimal approximation that is physically-realizable by the inverter. The controller is capable of compensating for the inherent delay of the system by employing appropriate prediction rules. Once an optimal input is synthesized, a voltage vector that best represents this input is selected and its associated switching state is sent to the inverter gates. The proposed control scheme draws upon the feedback-feedforward framework. As such, the back-EMF signal is treated as disturbance and is thus rejected by the closed-loop system. We show that a relatively more accurate prediction of the back-EMF signal (used within the formulated control law) can improve performance and robustness of the system.

Our main contribution is to provide an additional, computationally inexpensive, approach within the context of predictive current control of VSI's. In Section II the discrete-time model of the system is derived. Section III presents the delay-compensating deadbeat control law and its corresponding suboptimal voltage vector selection scheme. The effect of the back-EMF prediction is also discussed and a simple prediction rule that improves the robustness and performance of the system is proposed. Simulation results are given in Section IV. Concluding remarks are provided in Section V.

II. Discrete-Time Model

Fig. 1 depicts a generic closed-loop configuration of a current-regulated three-phase half-bridge VSI based on predictive current control methodology. The inverter is fed from a dc link voltage source V_{dc} and is connected to a balanced RL load in series with back-EMF voltages $\mathbf{e}$. The output voltage vectors generated by the inverter in terms of the phase to neutral voltages can be represented by

$$\mathbf{v} = \tfrac{2}{3}\left(v_{an} + \boldsymbol{\eta} v_{bn} + \boldsymbol{\eta}^2 v_{cn}\right), \quad \boldsymbol{\eta} := e^{j2\pi/3}. \qquad (1)$$

Combinations of the switching states of the inverter gate signals S_a, S_b, and S_c generate the following eight voltage

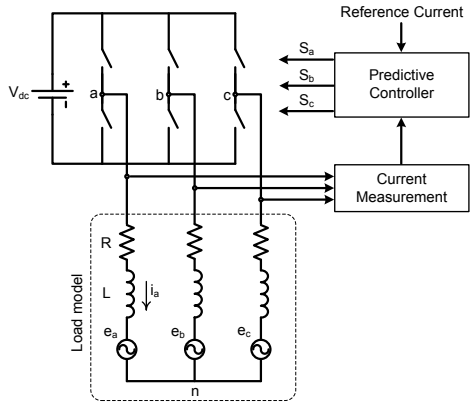

Fig. 1. Three-phase current-controlled VSI with RL load and back-EMF's

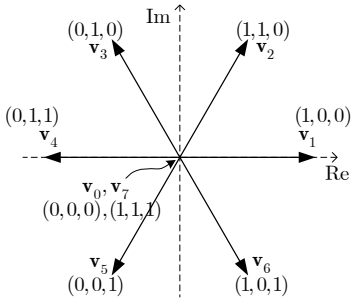

Fig. 2. Voltage vectors generated by the inverter. Respective switching states are also shown.

vectors across the load;

$$\mathbf{v}_\ell = \begin{cases} \frac{2}{3} V_{\text{dc}} e^{j(\ell-1)\pi/3} & \text{for} \quad \ell = \{1, \ldots, 6\} \\ \mathbf{0} & \text{for} \quad \ell = \{0, 7\}. \end{cases} \tag{2}$$

These vectors are shown in Fig. 2. The load current dynamics are then governed by the differential equation

$$\mathbf{v} = R\mathbf{i} + L\frac{d\mathbf{i}}{dt} + \mathbf{e} \tag{3}$$

with $\mathbf{i} = \frac{2}{3}\left(i_a + \boldsymbol{\eta} i_b + \boldsymbol{\eta}^2 i_c\right)$ and $\mathbf{e} = \frac{2}{3}\left(e_a + \boldsymbol{\eta} e_b + \boldsymbol{\eta}^2 e_c\right)$. Here, R and L are the load resistance and inductance, respectively.

To comply with the digital nature of the closed-loop system, we discretize (3) using the forward Euler method[1] by approximating the derivative term as $d\mathbf{i}/dt \approx \frac{1}{T}\left(\mathbf{i}(k+1) - \mathbf{i}(k)\right)$ where T is the sampling time. Therefore we obtain the following difference equation

$$\mathbf{i}(k+1) = A\mathbf{i}(k) + B\left\{\mathbf{v}(k) - \mathbf{e}(k)\right\} \tag{4}$$

with $A = 1 - TR/L$ and $B = T/L$.

III. The Proposed Predictive Controller

A. Deadbeat Control

We first seek an optimal deadbeat control law that if applied would eliminate the output error $\Delta_i := \mathbf{i} - \mathbf{i}^*$ at every time step k. Here "$*$" is to denote the reference signal.[2]

This control voltage is computed during the k^{th} sampling interval, i.e. $kT \le t \le (k+1)T$, and can only be applied at time instant $(k+1)T$. The output current affected by this control is then measured at the beginning of the $(k+2)^{\text{th}}$ sampling interval (see Fig. 3). Therefore there exists an inherent delay of two sampling intervals from the time a control is computed until the time the effect is sensed.

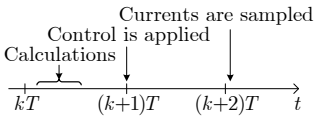

Fig. 3. The time-line of various events from the k^{th} sampling interval in which a control law is synthesized until its effect is sensed

To compensate for this time delay we compute the control input $\mathbf{u}^*(k+1)$ such that in (4) the commanding voltage (with a slight abuse of notation) is

$$\mathbf{v}(k) = z^{-1}\mathbf{u}^*(k+1) \tag{5}$$

where z^{-1} is the unit delay operator. Furthermore, by advancing (4) one time step such that $\mathbf{i}(k+2) = A\mathbf{i}(k+1) + B\{\mathbf{v}(k+1) - \mathbf{e}(k+1)\}$ and substituting for $\mathbf{i}(k+1)$ we can obtain, for a reference signal $\mathbf{i}^*(k+2)$, the following predictive control law;

$$\mathbf{u}^*(k+1) = \frac{1}{B}\Big[\mathbf{i}^*(k+2) - A\Big(A\mathbf{i}(k) + B\{\mathbf{v}(k) - z^{-1}\mathbf{e}(k+1)\}\Big)\Big] + \mathbf{e}(k+1). \tag{6}$$

Notice that in computation of $\mathbf{u}^*(k+1)$ in (6) during the k^{th} sampling interval, $\mathbf{i}(k)$ and $\mathbf{v}(k)$ are measured and available for use. On the other hand, $\mathbf{i}^*(k+2)$ and $\mathbf{e}(k+1)$ have to be predicted using previously acquired and/or estimated values. Henceforth we use the subscript "p" to denote a predicted signal. As such, a quadratic two-step-ahead prediction of the current reference can be computed from the Langrange extrapolation formula (see [2]) as

$$\mathbf{i}^*_p(k+2) = 6\mathbf{i}^*(k) - 8\mathbf{i}^*(k-1) + 3\mathbf{i}^*(k-2). \tag{7}$$

Similarly, the back-EMF voltage can be predicted as

$$\mathbf{e}_p(k+1) = 6\mathbf{e}(k-1) - 8\mathbf{e}(k-2) + 3\mathbf{e}(k-3) \tag{8}$$

where $\mathbf{e}(k-1)$ is estimated, at time step k, using

$$\mathbf{e}(k-1) = \frac{1}{B}\Big[A\mathbf{i}(k-1) - \mathbf{i}(k)\Big] + \mathbf{v}(k-1). \tag{9}$$

Assuming that there are no load parameter perturbations, it can be verified that if the predicted signals converge to their true values, i.e. $\mathbf{e}_p(k+1) = \mathbf{e}(k+1)$ and $\mathbf{i}^*_p(k+2) =$

[1]The forward Euler method provides sufficient accuracy if the sampling frequency is much larger than the fastest mode in the system, i.e. if the sampling period is sufficiently smaller than the time constant L/R.

[2]Our use of the term "optimal" is to refer to the fact that the deadbeat control law is the global minimizer of Δ_i. It follows that any approximation to this control law is decidedly suboptimal.

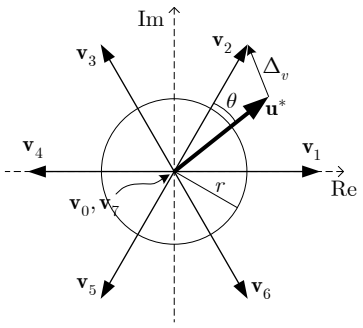

Fig. 4. Geometrical interpretation of the voltage vector selection scheme. The threshold r is a design parameter chosen as 40% or 50% of $|\mathbf{v}_\ell|$.

$\mathbf{i}^*(k+2)$, then the control law given in (6) constitutes a deadbeat policy since

$$\mathbf{i}(k+1) = A\mathbf{i}(k) + B\{z^{-1}\mathbf{u}^*(k+1) - \mathbf{e}(k)\} \quad (10)$$
$$= \mathbf{i}^*(k+1). \quad (11)$$

B. Suboptimal Voltage Vector Selection

The optimal control law (6) computed during the k^{th} sampling interval is an arbitrary complex quantity that cannot be directly generated by the inverter. Hence it must be approximated by the available voltage vectors $\mathbf{v}_\ell$, $\ell \in \{0, \ldots, 7\}$ ideally using a technique such as space vector modulation. As a result, multiple switching states are applied to the inverter gates during the next sampling interval. Naturally, this process is computationally burdensome and in some cases demands higher-than-needed switching frequency (albeit with the advantage of minimizing the Total Harmonic Distortion (THD) of the output current).

Instead, here we assume that the input voltage applied at every time step is to remain constant for the entire duration of the sampling interval and thus considerably reducing the computational costs. The synthesized predictive control law computed during the time interval $kT \le t \le (k+1)T$ is approximated by a single suboptimal voltage vector $\mathbf{v}_\ell$. This voltage is then applied to the load at time instant $(k+1)T$ until the next sampling interrupt. The selection of $\mathbf{v}_\ell$ at every time step can be formalized as follows

$$(\mathbf{v}_\ell|\mathbf{u}^*) : \ell = \begin{cases} \underset{\sigma\in\{1,\ldots,6\}}{\arg\min} \left| \cos^{-1}\left(\dfrac{\langle \mathbf{u}^*, \mathbf{v}_\sigma \rangle}{|\mathbf{u}^*| \cdot |\mathbf{v}_\sigma|} \right) \right|, & |\mathbf{u}^*| > r \\ 0, & |\mathbf{u}^*| \le r \end{cases} \quad (12)$$

where $\langle \cdot, \cdot \rangle$ denotes inner product. With $r = 0.5|\mathbf{v}_\ell|$ a voltage vector that satisfies (12) equivalently minimizes the error vector magnitude $|\Delta_v| := |\mathbf{v}_\ell - \mathbf{u}^*|$ (see Fig. 4).

Treated in polar coordinates, at any given time step, if the pre-computed $\mathbf{u}^*$ lies outside of a disc of radius r centered around the origin in the complex plane, then the non-zero voltage vector that constitutes the minimum angle with $\mathbf{u}^*$ is chosen as the suboptimal control input. Otherwise, the zero vector $\mathbf{v}_0$ is selected. Notice that $\mathbf{v}_0 = \mathbf{v}_7 = \mathbf{0}$ and therefore only seven vectors are considered in (12).

In practice, r can be chosen as $0.4|\mathbf{v}_\ell|$ in order to achieve lower THD for the output current. This however may cause steady-state error if the sampling frequency is not high enough.

The dependance of the output current THD on the choice of r may be explained by noticing the fact that the phase angle of the reference voltage $\mathbf{u}^*$ increases *almost* linearly (and periodically) with time. If at any given time step $\mathbf{u}^*(k)$ is located within the region in the complex plane bounded by any two adjacent nonzero vectors $\mathbf{v}_\imath$ and $\mathbf{v}_\jmath$, and $\ell = (\jmath \vee \imath)$ is found to be the solution of (12) at that time step, then it is likely that one of the same voltage vectors $\mathbf{v}_\imath$ or $\mathbf{v}_\jmath$ will be the solution at the next time step for the newly synthesized $\mathbf{u}^*$. This is true unless the magnitude of $\mathbf{u}^*$ is sufficiently small such that it can be best described by the zero voltage vectors. Setting the threshold to a slightly lower value $r = 0.4|\mathbf{v}_\ell|$ would then translate into selecting the zero vector fewer times than the case in which $r = 0.5|\mathbf{v}_\ell|$. Therefore the selection scheme is forced to have relatively fewer jumps to the origin when rotating among the regions in the complex plane. This in return results in comparatively lower THD of the output current.

Limiting (enforcing) the selection of the zero voltage vectors, however, must be performed with caution. Excessive reduction (increase) of the threshold value may lead to performance deterioration or instability under certain conditions. Moreover, this increase (decrease) in the on-time of the inverter in most cases will result in an adverse effect of magnifying higher order harmonics in the phase voltage waveform and thereby increasing the THD of the resulting output current. In our tests a radius value of $0.4|\mathbf{v}_\ell|$ has been found to yield the least current THD without causing significant steady-state error.

Notice that the inverter operates in saturation when the reference voltage $\mathbf{u}^*$ exceeds the hexagonal region comprised of the convex-hull of the vertices defined by the nonzero voltage vectors.

Once $\mathbf{v}_\ell$ is selected, the corresponding gate signal is directly sent to the inverter without the need for an intermediary circuit. In this case the commanding voltage (5) at time step k becomes $\mathbf{v}(k) = z^{-1}(\mathbf{v}_\ell|\mathbf{u}^*)(k+1)$. Substituting this in (4) and assuming as before that $\mathbf{e}_p(k+1) = \mathbf{e}(k+1)$ and $\mathbf{i}_p^*(k+2) = \mathbf{i}^*(k+2)$, we obtain the closed-loop equation as

$$\mathbf{i}(k+1) = A\mathbf{i}(k) + B\{z^{-1}(\mathbf{u}^*(k+1) + \Delta_v(k+1)) - \mathbf{e}(k)\} \quad (13)$$
$$= \mathbf{i}^*(k+1) + B\Delta_v(k). \quad (14)$$

It is clear that choosing a voltage vector that minimizes $|\Delta_v|$ minimizes the current error $|\Delta_i|$ at the next time step. Also notice that since $B = T/L$, choosing a smaller sampling interval has the effect of improving the closed-loop performance.

C. Back-EMF Prediction

As discussed before, for the optimal control law $\mathbf{u}^*$ in (6) to be realizable it must be approximated by the available

voltage vectors. Let us momentarily assume, for the sake of derivation of the closed-loop equations, that $\mathbf{u}^*$ is directly applied to the system. That is, we ignore the errors due to the approximation of $\mathbf{u}^*$.

To see the effect of back-EMF prediction on the dynamic response of the system we re-evaluate (10). In particular, using the Lagrange-based prediction (8) in (6) and substituting the results in (10) we can derive the closed-loop equation (with a loose exchange of notation between the time and frequency domains) as

$$\mathbf{i}(k+1) = \frac{1}{F_0(z)}\mathbf{i}^*(k+1) + \frac{D_0(z)}{F_0(z)}\mathbf{v}(k) \tag{15}$$

where

$$F_0(z) = \frac{1}{B}E_0(z)z^{-1} - \left(\frac{A}{B}E_0(z) - A^2\right)z^{-2} \tag{16}$$

$$D_0(z) = -B + (E_0(z) - BA)\,z^{-1} \tag{17}$$

$$E_0(z) = \left(Bz^{-1} + BAz^{-2}\right)\left[6 - 8z^{-1} + 3z^{-2}\right]. \tag{18}$$

Notice that in general the response of the filters $1/F_0(z)$ and $D_0(z)/F_0(z)$ alter according to the back-EMF prediction characterized by the bracketed term in $E_0(z)$. Specifically, for a perfect prediction, i.e. $\mathbf{e}_p(k+1) = \mathbf{e}(k+1) \equiv z^2\mathbf{e}(k-1)$, the term $1/F_0(z)$ has unity gain and zero phase-shift (with all the poles and zeros located at the origin) and the term $D_0(z)/F_0(z)$ has zero gain and zero phase-shift across all frequencies. In such a case, the closed-loop equation (15) reduces to (11) and the control (6) becomes a deadbeat policy. Therefore the desire for more accurate predictions of the back-EMF is evident.

For this purpose, while simultaneously aiming for real-time computational simplicity, we construct and employ a trivial 4-tap two-step-ahead finite impulse response (FIR) prediction filter so that the predicted back-EMF is

$$\mathbf{e}_p(k+1) = \sum_{n=0}^{3} \alpha_n \mathbf{e}(k-n-1). \tag{19}$$

Here the coefficients α_n are computed empirically and by taking advantage of some *a priori* knowledge about the shape of the back-EMF signal. These coefficients can be chosen such that the cut-off frequency of the FIR filter is well beyond the typical operating frequency range of VSI's and thus is applicable in various practical scenarios.

It can be shown that even with such simple prediction rule significant improvements in performance and robustness of the system can be achieved (see Sections III-D and IV).

With $R = 0.5\,\Omega$, $L = 10\,\text{mH}$, and $T = 100\,\mu\text{s}$, Fig. 5 compares the frequency responses of the input-output transfer function $1/F_0(z)$ for the Lagrange and FIR back-EMF predictions. It can be verified that the closed-loop response is closer to the ideal case (with perfect back-EMF prediction) when the FIR filter is used.

D. Robustness

It may be insightful to notice that the model-based predictive controller presented above has an inherent *feedforward* strategy to compensate for the input voltage disturbance (i.e.

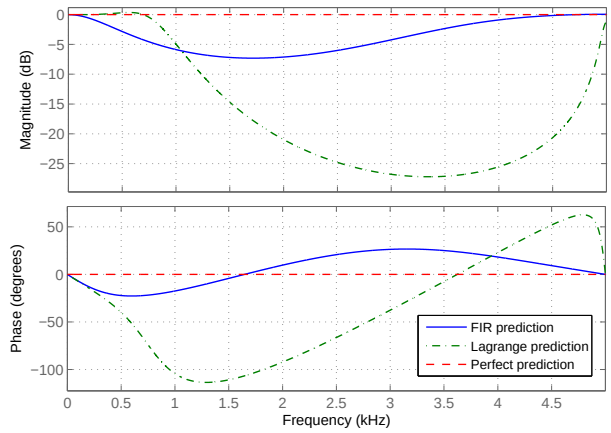

Fig. 5. Frequency response of $1/F_0(z)$ when perfect (dashed), FIR (solid), and Lagrange (dash-dotted) back-EMF predictions are used. Simulation parameters are $R = 0.5\,\Omega$, $L = 10\,\text{mH}$, and $T = 100\,\mu\text{s}$.

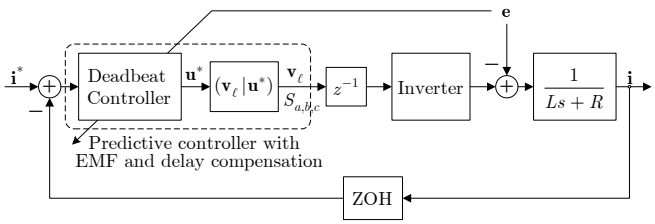

Fig. 6. Feedback-feedforward structure of the proposed predictive controller

the back-EMF $\mathbf{e}$). Within this framework the closed-loop system can be portrayed as in Fig. 6. It is clear that a controller that employs a more accurate back-EMF prediction does a better job at rejecting the disturbance.

In the presence of system parameter perturbation and model uncertainty the deviation in the system dynamics can be encapsulated to some extent by the disturbance signal $\mathbf{e}$. Therefore a more accurate prediction of the back-EMF voltage can account for some of the uncertainty and thus increase the overall robustness of the system. We will show this using an example in Section IV.

Notice that in this case the control law (6) becomes

$$\mathbf{u}^*(k+1) = \frac{1}{\widetilde{B}}\Big[\mathbf{i}^*(k+2) - \widetilde{A}\Big(\widetilde{A}\mathbf{i}(k) + \widetilde{B}\{\mathbf{v}(k) - z^{-1}\mathbf{e}(k+1)\}\Big)\Big] + \mathbf{e}(k+1) \tag{20}$$

where $\widetilde{A} := 1 - T\widetilde{R}/\widetilde{L}$ and $\widetilde{B} := T/\widetilde{L}$ are blind estimates of the true (possibly perturbed) system parameters A and B, respectively. The back-EMF voltage is now predicted according to

$$\mathbf{e}_p(k+1) = \Gamma(z)\widetilde{\mathbf{e}}(k-1) \tag{21}$$

where $\widetilde{\mathbf{e}}(k-1)$ is the estimated back-EMF using uncertain parameters and is computed as

$$\widetilde{\mathbf{e}}(k-1) = \frac{1}{\widetilde{B}}\Big[\widetilde{A}\mathbf{i}(k-1) - \mathbf{i}(k)\Big] + \mathbf{v}(k-1). \tag{22}$$

Here $\Gamma(z)$ characterizes the selected back-EMF prediction filter. For the FIR filter (19) this is $\Gamma(z) = \sum_{n=0}^{3} \alpha_n z^{-n}$. Substituting (20) in (10) (and ignoring the errors due to approximation of $\mathbf{u}^*$) we obtain the closed-loop equation as

$$\mathbf{i}(k+1) = \frac{B}{\widetilde{B}F(z)}\mathbf{i}^*(k+1) + \frac{D(z)}{F(z)}\mathbf{v}(k) \qquad (23)$$

with

$$F(z) = \frac{1}{\widetilde{B}}E(z)z^{-1} - \Big(\frac{\widetilde{A}}{\widetilde{B}}E(z) - \frac{BA^2}{\widetilde{B}}\Big)z^{-2} \qquad (24)$$

$$D(z) = -B + \Big(E(z) - B\widetilde{A}\Big)\, z^{-1} \qquad (25)$$

$$E(z) = \Big(Bz^{-1} + B\widetilde{A}z^{-2}\Big)\,\Gamma(z). \qquad (26)$$

Evidently, a perfect back-EMF prediction (which now encapsulates the effect of the uncertainty in the system) would be capable of entirely eliminating the effect of the parameter mismatch in (23).

Finally we point out that with a self-tuning adaptive scheme, such as the one proposed in [17], the model parameters and the back-EMF prediction converge to their true values in finite time. Therefore the robustness of the system is guaranteed and the closed-loop equation (23) reduces to (11) yielding a deadbeat control (albeit at the expense of added online computational complexity).

IV. Simulation Results

To evaluate the performance of the proposed predictive controller simulations are carried out using MATLAB/SIMULINK. The parameters are initially chosen according to

Case 1: $R = 0.5\,\Omega$, $L = 10\,\text{mH}$, $V_{\text{dc}} = 100\,\text{V}$
Case 2: $R = 10\,\Omega$, $L = 10\,\text{mH}$, $V_{\text{dc}} = 500\,\text{V}$.

A reference current with an amplitude of $13\,\text{A}$ and a frequency of $50\,\text{Hz}$ is to be tracked by the closed loop system. An unmeasurable sinusoidal disturbance (back-EMF) of fixed amplitude ($34\,\text{V}$) and frequency ($50\,\text{Hz}$) is applied to the system.

Primarily, to assess the performance of the proposed scheme, we compare the resulting phase-a load current with that obtained using the algorithm described in [15]. Note that in [15] the load model is discretized through *backward* Euler method and a voltage vector $\mathbf{v}_\ell$ that minimizes the cost functional $g = |i^*_\alpha(k+1) - i_\alpha(k+1)| + |i^*_\beta(k+1) - i_\beta(k+1)|$ (with $i_\alpha := \text{Re}(\mathbf{i})$ and $i_\beta := \text{Im}(\mathbf{i})$) is selected and applied to the load at every sampling instant. The output current is computed for all possible eight voltage vectors using $\mathbf{i}(k+1) = \frac{1}{RT+L}\left[L\mathbf{i}(k) + T\left(\mathbf{v}(k+1) - \mathbf{e}_p(k+1)\right)\right]$ where the back-EMF is assumed to be constant over a sampling period and is thus predicted using $\mathbf{e}_p(k+1) \approx \mathbf{e}(k) = \mathbf{v}(k) + \frac{L}{T}\mathbf{i}(k-1) - \frac{RT+L}{T}\mathbf{i}(k)$.

Figs. 7 and 8 show the phase-a load current obtained using the proposed predictive controller (top plots in each figure) vs. that obtained using the predictive algorithm [15] (bottom plots in each figure) for parameter values in Case 1 and 2, respectively. A sampling period of $T = 100\,\mu\text{s}$ has been used and a voltage selection radius of $r = 0.4|\mathbf{v}_\ell|$ in (12) has been chosen. It can be observed that the current ripples are significantly reduced when our proposed controller is in use. Table I quantifies the Total Harmonic Distortion (THD) of the steady-state output current for each controller with two sampling intervals $T = 100\,\mu\text{s}$ and $T = 20\,\mu\text{s}$. It can be noticed that by using the proposed predictive controller up to 60% reduction in THD can be achieved while the steady-state and transient responses are also improved.

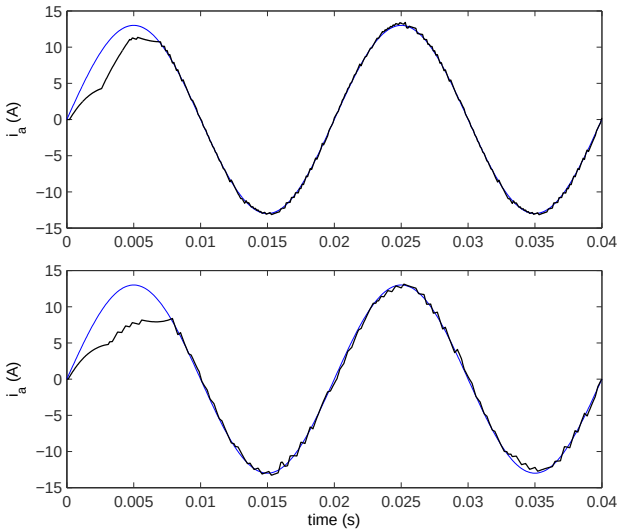

Fig. 7. Phase-a response with parameter values in Case 1 and $T = 100\,\mu\text{s}$. Top: using the proposed controller. Bottom: using the algorithm in [15].

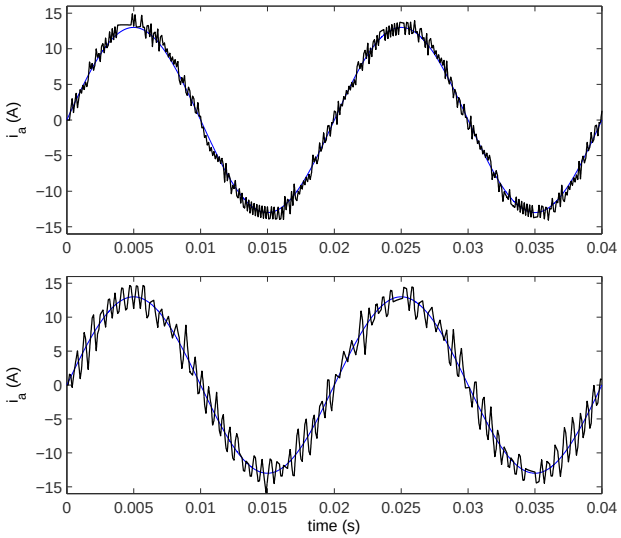

Fig. 8. Phase-a response with parameter values in Case 2 and $T = 100\,\mu\text{s}$. Top: using proposed controller. Bottom: using the algorithm in [15].

Fig. 9 shows the response of the closed-loop system to step changes in the reference current. The simulation parameters are chosen according to Case 1 with $T = 100\,\mu\text{s}$. At $t = 0.024\,\text{s}$ the amplitude of both the real and the imaginary components of $\mathbf{i}^*$ are reduced to $5\,\text{A}$. At $t = 0.033\,\text{s}$ the amplitude of the real component of $\mathbf{i}^*$ is further reduced to

TABLE I

OUTPUT CURRENT THD WHEN USING THE PROPOSED PREDICTIVE CONTROLLER VS. THE ALGORITHM IN [15].

	THD using the proposed controller	**THD using the controller in [15]**
Case 1 ($T = 100\,\mu$s)	1.47%	3.23%
Case 2 ($T = 100\,\mu$s)	6.68%	15.44%
Case 1 ($T = 20\,\mu$s)	0.33%	0.71%
Case 2 ($T = 20\,\mu$s)	1.41%	3.54%

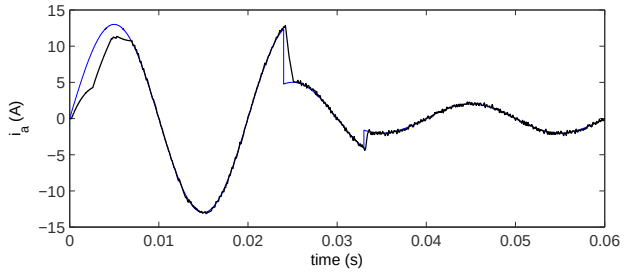

Fig. 9. Phase-a response to step changes in the reference current. Parameters are chosen according to Case 1 and $T = 100\,\mu$s.

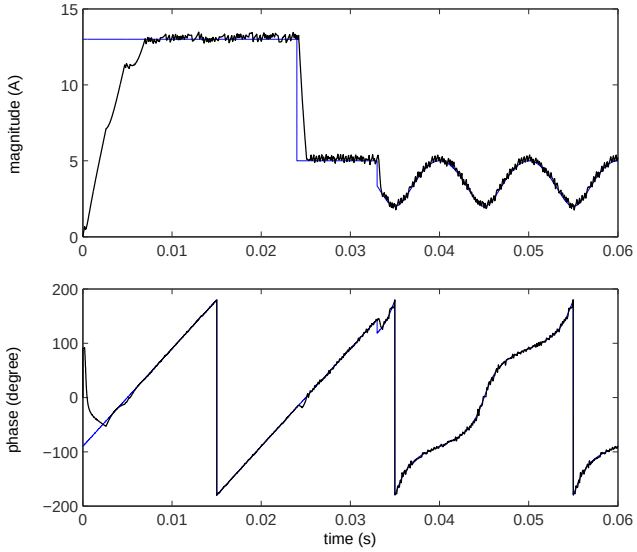

Fig. 10. The magnitude (top) and phase (bottom) of the output current $\mathbf{i}$ in response to various step changes in imaginary and real components of $\mathbf{i}^*$. Parameters are according to Case 1 and $T = 100\,\mu$s.

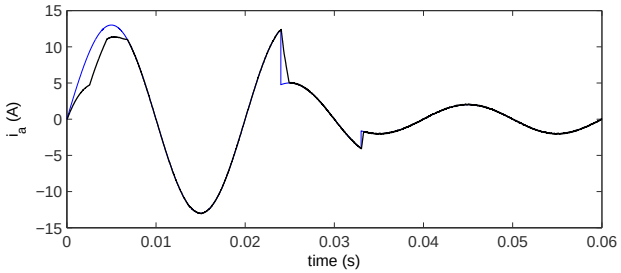

Fig. 11. Phase-a response to step changes in the reference current. Parameters are chosen according to Case 1 and $T = 20\,\mu$s.

2 A while keeping the imaginary component fixed. Fig. 10 shows the magnitude and phase of the output current $\mathbf{i}$.

It is shown in Fig. 11 that smaller sampling interval ($T = 20\,\mu$s) yields a more profound separation between the fundamental and higher order harmonics. In such a case an even better transient response and steady-state tracking can be achieved.

A. Effect of Back-EMF Prediction on Performance

Fig. 12 shows the response of the closed-loop system to step changes in the reference current when the parameters of the system are chosen according to Case 2 with sampling interval $T = 100\,\mu$s. Notice that thus far the back-EMF has been predicted using an FIR prediction filter as described in Section III-C with coefficients $\alpha_0 = 0.5337$, $\alpha_1 = 0.3636$, $\alpha_2 = 0.0926$, $\alpha_3 = 0.0081$. In comparison, Fig. 13 shows the response when a Lagrange back-EMF prediction is employed. Clearly a better performance is achieved when the FIR prediction filter is in use.

The THD of the output current in steady-state for the FIR back-EMF prediction (when $\mathbf{i}^*$ is simply a sinusoidal signal with 13 A amplitude and 50 Hz frequency) is 6.68% whereas employing a Lagrange prediction rule increases the THD to 8.05%. For this case Figs. 14 and 15 show the FIR and Lagrange back-EMF predictions, respectively.

B. Robustness

1) Parameter Mismatch: Fig. 16 shows the Mean Squared Error (MSE) of the phase-a current in steady-state in the presence of model uncertainty when FIR and Lagrange back-EMF predictions are employed. The nominal (true) values are set according to Case 1 and the sampling interval is $T = 100\,\mu$s. It is clear that when the more accurate FIR back-EMF prediction is employed the closed-loop system is capable of tolerating a wide range of parameter mismatch. On the other hand when the Lagrange back-EMF prediction is used the error in the response increases rapidly when the induction value deviates from its nominal value, ultimately resulting in instability.

Fig. 17 shows the phase-a response with $\Delta L(:= \frac{\tilde{L}}{L} - 1) = -60\%$ when FIR and Lagrange back-EMF predictions are used. The nominal values are chosen according to Case 1 and the sampling interval is $T = 100\,\mu$s. Improved performance of the closed-loop system with FIR prediction in the presence of uncertainty can be clearly observed.

2) Parameter Perturbation: The top plot in Fig. 18 shows the phase-a response of the closed-loop system with the proposed controller when the system parameters are perturbed at $t = 0.025$ s. Here the load inductance L is suddenly dropped to 20% of its nominal value (as given in Case 1) while the load resistance R is raised by 80%. The sampling interval is chosen as $T = 20\,\mu$s. In comparison, the performance of the control algorithm presented in [15] is severely degraded under the same conditions as shown in the bottom plot of Fig. 18.

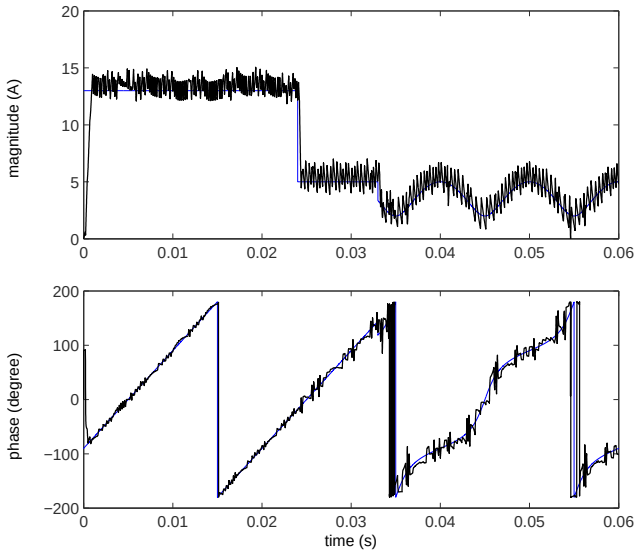

Fig. 12. The magnitude (top) and phase (bottom) of the output current $\mathbf{i}$ in response to step changes in $\mathbf{i}^*$. Parameters are according to Case 2 and $T = 100\,\mu$s. (FIR back-EMF prediction).

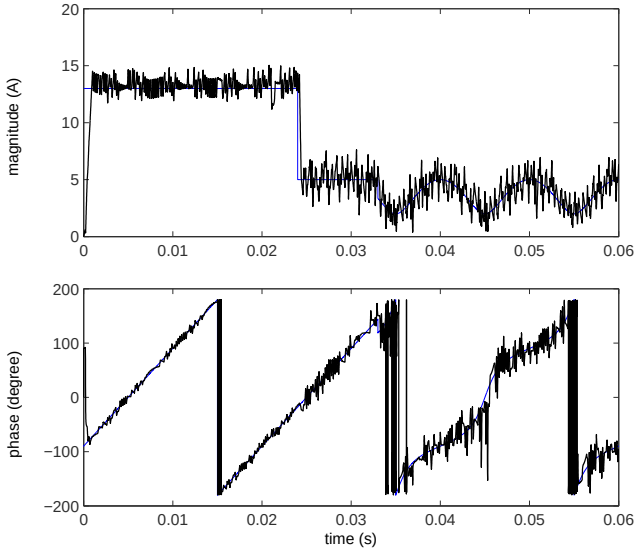

Fig. 13. The magnitude (top) and phase (bottom) of the output current $\mathbf{i}$ in response to step changes in $\mathbf{i}^*$. Parameters are according to Case 2 and $T = 100\,\mu$s. (Lagrange back-EMF prediction)

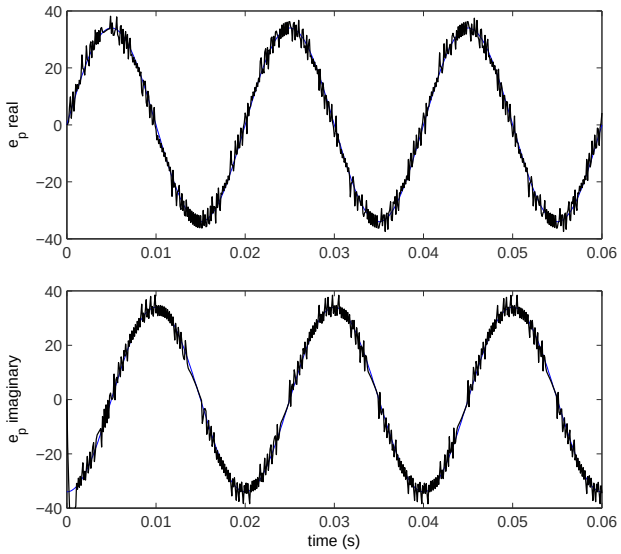

Fig. 14. Predicted back-EMF voltage (using FIR prediction) for a current reference $\mathbf{i}^*$ with fixed amplitude (13 A) and frequency (50 Hz).

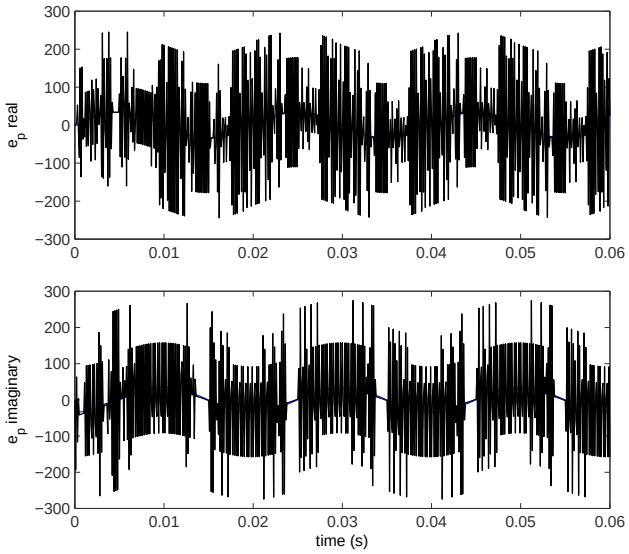

Fig. 15. Predicted back-EMF voltage (using Lagrange prediction) for a current reference $\mathbf{i}^*$ with fixed amplitude (13 A) and frequency (50 Hz).

V. Conclusions

In this paper we presented a predictive current control strategy for a voltage-source inverter. A discretized load model was obtained using forward Euler method. A deadbeat control law based on this model was formulated. This optimal control policy, computed at every sampling interval, would eliminate the output current error while compensating for the inherent delay associated with the closed-loop system. A selection scheme was proposed that approximates the control input with the most appropriate (suboptimal) voltage vector. It was also shown that the selection scheme can be modified to reduce the current ripples at the output of the system. Once a voltage vector is selected its corresponding switching state is sent directly to the inverter gates without the need for an intermediary circuit.

It was argued that the proposed scheme can be best described within the feedback-feedforward framework in which the induced back-EMF voltage across the load is treated as disturbance. Since the proposed controller relies on the predictions of the back-EMF signal, discussions surrounding the effect of this prediction on the performance and robustness of the system was provided. It was shown that the use of a simple but relatively more accurate prediction filter (as opposed to the commonly used polynomial rules) can greatly improve the performance and robustness of the system.

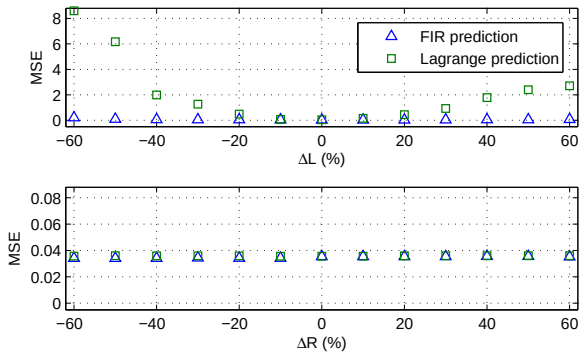

Fig. 16. Mean Squared Error (MSE) of the phase-a current in steady-state when FIR and Lagrange back-EMF predictions are employed versus parameter uncertainty $\Delta L := \widetilde{L}/L - 1$ and $\Delta R := \widetilde{R}/R - 1$. Here R and L are the true variables and $\widetilde{R}$ and $\widetilde{L}$ are their corresponding blind estimates used for control synthesis.

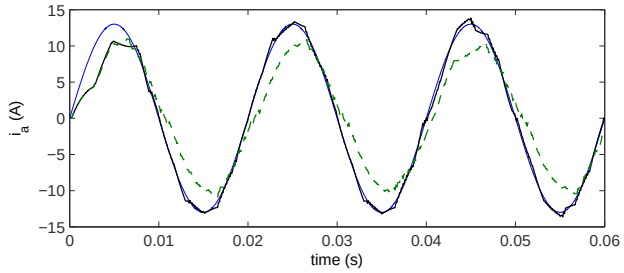

Fig. 17. Phase-a response with $\Delta L = -60\%$ when FIR (solid) and Lagrange (dashed) back-EMF predictions are employed.

Simulations were provided for two nominal configurations. The performance of the system was compared to the algorithm presented in [15] as a point of reference. The effect of back-EMF prediction was also studied using a number of examples. Finally, the robustness of the system to parameter perturbation and model uncertainty was assessed.

Future work may include modification to the control strategy such that the changes in the active and reactive components of the output current are decoupled.

REFERENCES

[1] P. Cortes, M. P. Kazmierkowski, R. M. Kennel, D. E. Quevedo, and J. Rodriguez, "Predictive control in power electronics and drives," *IEEE Transactions on Industrial Electronics*, vol. 55, no. 12, pp. 4312–4324, Dec. 2008.

[2] O. Kükrer, "Discrete-time current control of voltage-fed three-phase PWM inverters," *IEEE Transactions on Power Electronics*, vol. 11, no. 2, pp. 260–269, 1996.

[3] G. Bode, P. Loh, M. Newman, and D. Holmes, "An improved robust predictive current regulation algorithm," in *Proc. International Conference on Power Electronics and Drive Systems*, vol. 2, 2003.

[4] T. Habetler, "A space vector-based rectifier regulator for AC/DC/AC converters," *IEEE Transactions on Power Electronics*, vol. 8, no. 1, pp. 30–36, 1993.

[5] R. Kennel, A. Linder, and M. Linke, "Generalized predictive control (GPC)-ready for use in drive applications?" in *Proc. IEEE Power Electronics Specialists Conference*, vol. 4, Vancouver, Canada, 2001, pp. 1839–1844.

[6] L. Malesani, P. Mattavelli, and S. Buso, "Robust dead-beat current control for PWM rectifiers and active filters," *IEEE Transactions on Industry Applications*, vol. 35, no. 3, pp. 613–620, 1999.

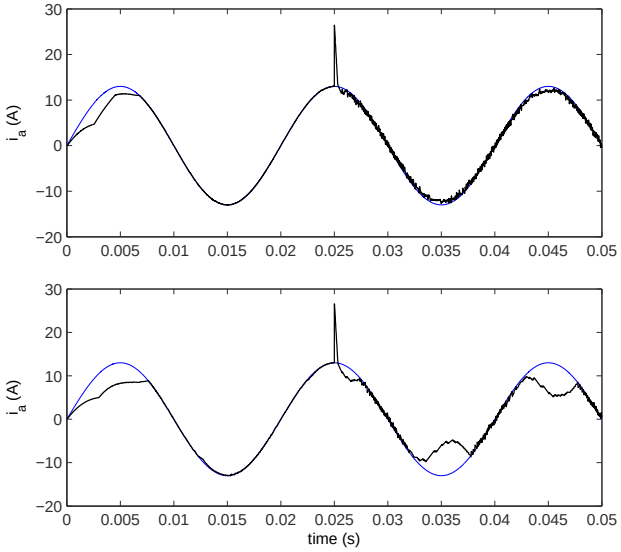

Fig. 18. Phase-a response of the system with a sudden parameter perturbation of the load. Top: using the proposed controller (with FIR back-EMF prediction). Bottom: using the algorithm in [15].

[7] R. Wu, S. Dewan, G. Slemon, I. Ltd, and O. Burlington, "Analysis of an AC-to-DC voltage source converter using PWM with phase and amplitude control," *IEEE Transactions on Industry Applications*, vol. 27, no. 2, pp. 355–364, 1991.

[8] P. Mattavelli, G. Spiazzi, and P. Tenti, "Predictive digital control of power factor preregulators with input voltage estimation using disturbance observers," *IEEE Transactions on Power Electronics*, vol. 20, no. 1, pp. 140–147, 2005.

[9] S. Saggini, W. Stefanutti, E. Tedeschi, and P. Mattavelli, "Digital deadbeat control tuning for dc-dc converters using error correlation," *IEEE Transactions on Power Electronics*, vol. 22, no. 4, pp. 1566–1570, 2007.

[10] R. Wu, S. Dewan, and G. Slemon, "A PWM AC-to-DC converter with fixed switching frequency," *IEEE Transactions on Industry Applications*, vol. 26, no. 5, pp. 880–885, 1990.

[11] H. Abu-Rub, J. Guzinski, Z. Krzeminski, and H. A. Toliyat, "Predictive current control of voltage-source inverters," *IEEE Transactions on Industrial Electronics*, vol. 51, no. 3, pp. 585–593, 2004.

[12] H. Kojabadi, B. Yu, I. Gadoura, L. Chang, and M. Ghribi, "A novel DSP-based current-controlled PWM strategy for single phase grid connected inverters," *IEEE transactions on power electronics*, vol. 21, no. 4, pp. 985–993, 2006.

[13] E. Wu and P. Lehn, "Digital current control of a voltage source converter with active damping of LCL resonance," *IEEE Transactions on Power Electronics*, vol. 21, no. 5, pp. 1364–1373, 2006.

[14] A. Nasiri, "Digital control of three-phase series-parallel uninterruptible power supply systems," *IEEE Transactions on Power Electronics*, vol. 22, no. 4, pp. 1116–1127, 2007.

[15] J. Rodriguez, J. Pontt, C. A. Silva, P. Correa, P. Lezana, P. Cortes, and U. Ammann, "Predictive current control of a voltage source inverter," *IEEE Transactions on Industrial Electronics*, vol. 54, pp. 495–503, Feb. 2007.

[16] H. Moon, H. Kim, and M. Youn, "A discrete-time predictive current control for PMSM," *IEEE Transactions on Power Electronics*, vol. 18, no. 1, pp. 464–472, 2003.

[17] Y. A.-R. I. Mohamed and E. F. El-Saadany, "An improved deadbeat current control scheme with a novel adaptive self-tuning load model for a three-phase PWM voltage-source inverter," *IEEE Transactions on Industrial Electronics*, vol. 54, pp. 747–759, 2007.